

Evolution of electronic states in $R\text{CoO}_3$ (R =rare earth): Heat capacity measurements

Makoto Tachibana,¹ Takahiro Yoshida,² Hitoshi Kawaji,² Tooru Atake,² and Eiji Takayama-Muromachi³

¹ICYS, National Institute for Materials Science, Namiki 1-1, Tsukuba, Ibaraki 305-0044, Japan

²Materials and Structures Laboratory, Tokyo Institute of Technology, 4259 Nagatsuta-cho, Midori-ku, Yokohama 226-8503, Japan

³Advanced Nano Materials Laboratory, National Institute for Materials Science, Namiki 1-1, Tsukuba, Ibaraki 305-0044, Japan

(Received 22 November 2007; revised manuscript received 11 January 2008; published 5 March 2008)

The electronic phase diagram of $R\text{CoO}_3$ (R =rare-earth) perovskites has been mapped out through high-pressure synthesis and heat capacity (C_p) measurements. In contrast to $R=\text{La}$ where the spin-state transition and insulator-metal transition each shows a broad C_p anomaly, these anomalies merge into a large C_p peak for smaller R . A detailed structural study employing synchrotron x-ray powder diffraction shows that the onset temperature for the spin-state transition is correlated with the σ^* -bonding e_g bandwidth. A possible scenario on the spin state is provided to explain the C_p anomaly and phase diagram.

DOI: 10.1103/PhysRevB.77.094402

PACS number(s): 75.30.Wx, 65.40.Ba, 71.30.+h, 75.40.Cx

I. INTRODUCTION

The nature of spin-state and insulator-metal (IM) transitions in perovskite $R\text{CoO}_3$, where R is a trivalent rare earth, remains one of the most intriguing problems posed by transition metal oxides. In addition to the intricate interplay between charge, spin, and orbital degrees of freedom, which is a characteristic of strongly correlated oxides, the cobaltates show thermal excitations of spin states. As a result, interpretation of the electronic phenomena requires some assumptions on the spin state, while identifying the spin state requires detailed and precise understanding of the electronic phenomena. This predicament has resulted in long-standing controversy, the history of which goes back to the 1950s (Ref. 1) and still continues today. In $R\text{CoO}_3$, the ground state of the localized Co^{3+} ions is the nonmagnetic $S=0$ that corresponds to the low-spin (LS) $t_{2g}^6 e_g^0$ configuration. As the crystal-field splitting Δ_{CF} between the t_{2g} and e_g states is only slightly larger than the Hund coupling energy, the system can be thermally excited to either a high-spin (HS) ($S=2$; $t_{2g}^4 e_g^2$) or an intermediate-spin (IS) ($S=1$; $t_{2g}^5 e_g^1$) configuration. For $R=\text{La}$, which has the largest ionic radius among the rare earth (see Fig. 1), the signature for the onset of spin-state transition at $T_{\text{onset}} \sim 35$ K is seen in the magnetic susceptibility,²⁻⁴ heat capacity,^{3,5} and thermal expansion.⁴ Identifying the excited state is difficult, however, since the analysis requires various assumptions on degeneracy, spin-orbit coupling, and activation energy. With increasing temperature T , the magnetic susceptibility first shows a broad peak at ~ 100 K.²⁻⁴ This peak is not accompanied by anomaly in other thermodynamic measurements,^{3,4} implying that the spin-state transition is associated with thermal excitations and not a phase transition. Around 530 K, the phase transition to a metallic phase is marked by distinct anomaly in the magnetic susceptibility,^{4,6} resistivity,⁷ heat capacity,⁵ and thermal expansion.⁶ Following the results of band-structure calculations,⁸ a number of studies supported the IS state as the first excited-spin state, with the IM transition possibly accompanied by additional transition to the HS state.^{6,9} However, this scenario is not consistent with some experiments, most notably the electron spin resonance¹⁰ and heat capacity.³ A series of recent

studies^{3,11,12} showed that a consistent picture can be achieved by excitations to a triply degenerate HS state, where the activation energy *increases* with increasing HS population. Within this picture, the system is in an inhomogeneous mixed-spin state at room temperature, possibly transforming to an IS state above the IM transition.^{3,13}

Substitution of smaller R for $R=\text{La}$ increases the cooperative rotations of the corner-sharing CoO_6 octahedra, reducing the Co-O-Co bond angles and the bandwidth of Co($3d$)-O($2p$) interactions. This feature of the perovskite structure suggests that better understanding of the spin-state and IM transitions may be achieved through systematic studies as a function of the ionic radius of $R(r_R)$. Indeed, an

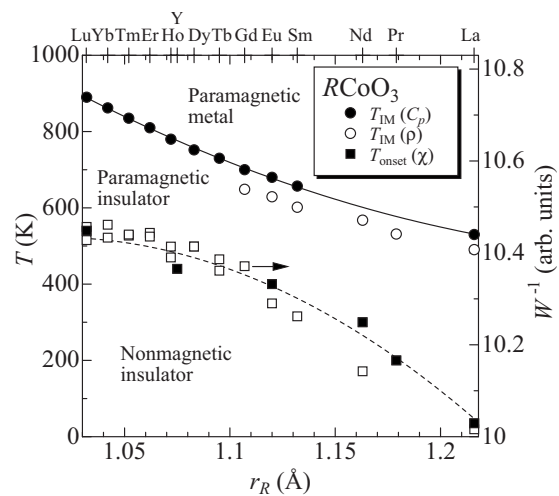


FIG. 1. The electronic phase diagram for $R\text{CoO}_3$ as a function of the ionic radius $R(r_R)$. The solid squares are the onset temperatures for the spin-state transition determined from magnetic susceptibility. Sources are $R=\text{La}$, Pr, and Nd (Ref. 2), $R=\text{Eu}$ (Ref. 14), and $R=\text{Y}$ and Lu (Ref. 15). The open squares are the inverse of bandwidth W^{-1} , obtained from the structural parameters. The open and filled circles represent the insulator-metal transition temperatures determined from heat capacity [$R=\text{La}$ (Ref. 5); others, this study] and resistivity (Ref. 16), respectively. The latter may depend on sample quality as $T_{\text{IM}}(\rho) \sim T_{\text{IM}}(C_p)$ is evident for $R=\text{La}$ in Ref. 7.

examination of the literature^{2,14,15} shows that the onset temperature T_{onset} for the spin-state transition increases with decreasing r_R , as displayed in Fig. 1. [The values for $R=\text{Pr}$, Nd ,² and Eu (Ref. 14) were obtained by subtracting the rare-earth contributions.] Since T_{onset} measures the size of the spin gap, Fig. 1 demonstrates the effect of reducing r_R on the stability of the nonmagnetic LS state. Similarly, the resistivity studies¹⁶ on $R=\text{La-Gd}$ single crystals found that T_{IM} increases with decreasing r_R (Fig. 1), showing an important role of r_R on the IM transition. However, whether there exists a single parameter that determines the magnitude of both T_{onset} and T_{IM} , or there are more complex yet explicit relationships between the two transitions, remain unclear for the following reasons: Structural parameters are not available for the intermediate-sized $R=\text{Sm}$, Eu , and Gd with strong neutron absorption,¹⁷ and the synthesis becomes increasingly difficult for small R . Moreover, resistivity measurements become less reliable for these compounds where single crystals or sintered pellets cannot be prepared readily. In this study, we provide the complete picture by performing heat capacity and synchrotron x-ray powder diffraction measurements on the series of $R\text{CoO}_3$ compounds prepared under high pressure. The results clarify the bandwidth dependence of the spin-state transition, while the IM transition can be explained with the stabilization of a homogeneous IS state at high T .

II. EXPERIMENT

$R\text{CoO}_3$ ($R=\text{Sm}$, Eu , Gd , Tb , Dy , Ho , Er , Tm , Yb , and Lu) were prepared under high-pressure conditions. Appropriate quantities of $R_2\text{O}_3$, Co_3O_4 , and KClO_4 (oxygen source) were mixed together and sealed in a gold capsule. The capsule was heated to 1723 K for 3 h at 6 GPa in a belt-type press and rapidly cooled to room temperature before releasing the pressure. The products were composed of small ($<100 \mu\text{m}$) crystallites, and KCl was removed by washing with distilled water. Phase purity of the crystallites was confirmed by powder x-ray diffraction. Heat capacity data from 300 to 1000 K were obtained by the enthalpy method¹⁸ using a Perkin Elmer differential scanning calorimeter. The sample weighing ~ 30 mg was set in a covered gold pan, and the measurements were performed in flowing air. The accuracies of the measurement are approximately 0.3% at 400 K and 1% at 1000 K.^{18,19} Synchrotron x-ray powder diffraction measurements were performed at 300 K on the BL02B2 beamline at SPring-8 using a wavelength of 0.4 Å. Structural parameters in the orthorhombic space group $Pbnm$ were refined by the Rietveld method using the program RIETAN-2000.²⁰ Good reliability factors similar to those of our previous studies on RMnO_3 (Ref. 21) were obtained.²²

III. RESULTS AND DISCUSSION

Figure 2 shows the room-temperature variation of the lattice parameters a , b , and c , volume V , the average Co-O bond distance $\langle\text{Co-O}\rangle$, and the average Co-O-Co bond angle $\langle\theta\rangle$ as a function of r_R . In $R\text{CoO}_3$, splitting of each bond distance and bond angle from the average value is very small ($<1.1\%$ and $<0.6\%$, respectively¹⁷) and is not shown in the

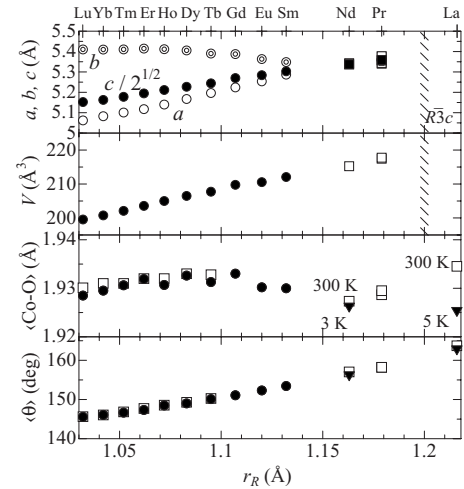


FIG. 2. The room-temperature values of the lattice parameters, volume, average Co-O bond distance $\langle\text{Co-O}\rangle$, and average Co-O-Co bond angle $\langle\theta\rangle$ as a function of r_R . Circles are the present synchrotron x-ray data, while squares are from neutron data. [Sources: $R=\text{La}$ (Ref. 9), $R=\text{Pr}$ (Refs. 17 and 23), $R=\text{Nd}$ (Ref. 24), and $R=\text{Tb-Lu}$ (Ref. 17).] For a , b , c , V , and each θ , error bars are smaller than the symbols. Error bars for each Co-O are about ± 0.002 Å in the present data. For $R=\text{La}$ and Nd , low-temperature values are also shown with inverted triangles.

figure. Both the present synchrotron x-ray (filled circle) and earlier neutron^{9,17,23,24} (empty square) data are presented for $\langle\text{Co-O}\rangle$ and $\langle\theta\rangle$, showing good agreement between the two techniques. With increasing r_R , V is increased continuously while the orthorhombic splitting with $b > c/\sqrt{2} > a$ is reduced progressively, becoming pseudocubic at $R=\text{Nd}$ and then turning to $a > c/\sqrt{2} > b$ for $R=\text{Pr}$ before transforming to the rhombohedral $R\bar{3}c$ structure in $R=\text{La}$. Similar behavior is observed in rare-earth perovskites in general and RNiO_3 in particular,²⁵ where the latter also shows an orthorhombic to rhombohedral transition between $R=\text{Pr}$ and La . The increasing rotation of the CoO_6 octahedra with decreasing r_R reduces $\langle\theta\rangle$ from 180° in the ideal cubic perovskite to 164° – 146° in $R\text{CoO}_3$, as is seen in Fig. 2. On the other hand, $\langle\text{Co-O}\rangle$ remains almost constant except for $R=\text{La}$, with a broad maximum at $r_R \sim 1.1$ Å. To examine how the spin-state transition affects the structural parameters, the low- T values of $\langle\text{Co-O}\rangle$ and $\langle\theta\rangle$ for $R=\text{Nd}$ (at 3 K) and La (5 K) are also shown in Fig. 2. For $R=\text{Nd}$ (and for smaller R), Fig. 1 indicates that Co^{3+} is in the LS state below 300 K, so the small difference in $\langle\text{Co-O}\rangle$ and $\langle\theta\rangle$ between 3 and 300 K reflects the conventional thermal expansion within the LS state. On the other hand, a large fraction of the Co^{3+} spins is already excited at 300 K for $R=\text{La}$, which explains the significant increase in $\langle\text{Co-O}\rangle$ between 5 and 300 K. The spin-state transition appears to have a much smaller effect on $\langle\theta\rangle$, as its increase is similar in $R=\text{La}$ and Nd . For $R=\text{Pr}$, $T_{\text{onset}} \sim 200$ K makes the room-temperature value an average of a majority of LS and a small fraction of excited spins.

The small change in $\langle\text{Co-O}\rangle$ for the series of $R\text{CoO}_3$ implies that the stabilization of the LS state with decreasing r_R is not due to an increase in Δ_{CF} , as occurs under hydrostatic

pressure.^{26,27} Thus, taking into account that the Hund coupling energy is also practically invariant for the series of $R\text{CoO}_3$, the spin gap should be most sensitive to a change in the σ^* -bonding e_g bandwidth W .²⁷ As the broadening of W reduces the spin gap and T_{onset} , this relationship can be tested explicitly by comparing T_{onset} and W^{-1} (or $-W$) for the series of $R\text{CoO}_3$. Moreover, the availability of structural parameters for each R allows the calculation of W through $W \propto \cos \omega / \langle \text{Co-O} \rangle^{3.5}$, where $\omega = (180 - \langle \theta \rangle) / 2$ is the tilting angle of the CoO_6 octahedra.²⁸ Except for $R=\text{La}$ and Pr , we use the room-temperature values to obtain W^{-1} for the LS state. Fortunately, the comparison between the 3 and 300 K values for $R=\text{Nd}$ shows that the increase in $\langle \theta \rangle$ offsets the increase in $\langle \text{Co-O} \rangle$ to give practically a T -independent W^{-1} (10.136 at 3 K and 10.142 at 300 K) within the LS state. This indicates that the 5 K data for $R=\text{La}$ provide the LS W^{-1} value that can be compared with other R . The results are presented in Fig. 1 with the scale shown in the unit of $\text{\AA}^{3.5}$; the strong correlation between W^{-1} and T_{onset} clarifies the direct role of σ^* -bonding bandwidth on the spin gap. Interestingly, plotting $-W$ gives the same r_R dependence as W^{-1} , suggesting that the spin gap may be directly associated with $\Delta_{\text{CF}} - W/2$.²⁷ Moreover, $R=\text{La}$ appears to be on the verge of critical region where a small increase in W may push T_{onset} to 0 K.

Since the evolution of W^{-1} with r_R is steric in origin [similar evolution is found in $R\text{FeO}_3$ (Ref. 29)], it may be applied to other perovskite series. For example, $R\text{NiO}_3$ shows an IM transition where T_{IM} evolves in a manner similar to T_{onset} in $R\text{CoO}_3$.³⁰ Although structural analysis in $R\text{NiO}_3$ is complicated by the presence of charge segregation in the insulating phase, these similarities suggest that T_{IM} in $R\text{NiO}_3$ is also related to the e_g -derived bandwidth for the series of R .³¹

Having established the bandwidth dependence of spin-state transition, we now expand the scope of our discussion to include the IM transition. In Fig. 3, the high- T ($T > 300$ K) heat capacity C_p is shown, where the previous result⁵ for $R=\text{La}$ is also plotted. For each R , the most prominent feature is the peak at the IM transition. Here, T_{IM} systematically increases with decreasing r_R , mapping the phase boundary for the entire series in Fig. 1. Note that T_{IM} evolves in a manner different from W^{-1} , implying that the IM transition is not a simple Mott transition with the bandwidth being the sole parameter. To gain better perspectives on the electronic transitions, we plot the data in C_p/T for $R=\text{La}$, Gd , and Lu in Fig. 4. These compounds are selected since the analysis is not complicated by contributions from rare-earth crystal-field excitations, allowing direct examination of Co^{3+} entropy by integrating the excess part of C_p/T . Here, the baseline (thick line) can be established by an extrapolation using the value of $R=\text{Lu}$ below $T_{\text{onset}}=540$ K, which smoothly converges with the data for $R=\text{La}$ above 900 K and also with the extrapolated data for $R=\text{Gd}$ and Lu at higher T .³² At 300 K, C_p/T for $R=\text{La}$ is larger than $R=\text{Gd}$ and Lu by $0.03 \text{ J K}^{-2} \text{ mol}^{-1}$, which agrees with the excess $\Delta C_p/T$ for $R=\text{La}$ obtained in Ref. 3 and reproduced in the inset. For $R=\text{La}$, there is a strong resemblance between $\Delta C_p/T$ and the thermal expansion,⁴ where the onset of spin-

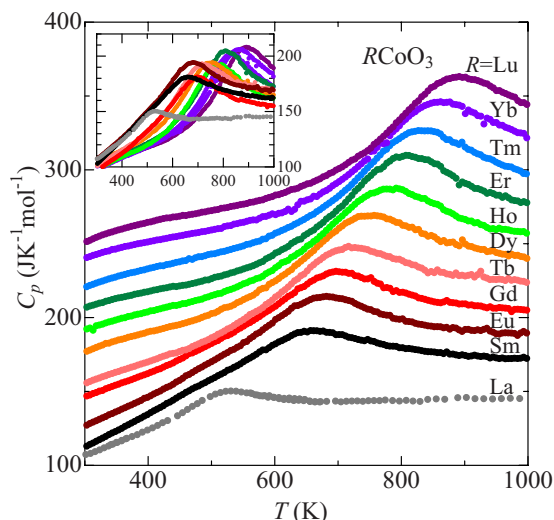


FIG. 3. (Color online) The heat capacity of $R\text{CoO}_3$ between 300 and 1000 K. The data for $R=\text{La}$ are obtained from Ref. 5. The data have been offset by 0, 10, 20, 50, 55, 75, 95, 105, 125, 140, and 155 $\text{J K}^{-1} \text{ mol}^{-1}$, respectively, for clarity. The inset shows the same data without the offset.

state transition is followed by a peak at 50 K. Here, $\Delta C_p/T$ maintains a finite and almost constant value for 200–400 K, indicating that contributions from spin-state transition persist in this temperature region. At higher T , contributions from IM transition become dominant until the excess contribution diminishes at ~ 900 K. Overall, the results demonstrate the successive evolution of electronic states for $R=\text{La}$, with the total excess entropy of $26 \text{ J K}^{-1} \text{ mol}^{-1}$. While separate contributions from the spin-state and IM transitions were also observed in the thermal expansion³³ for $R=\text{Pr}$ and Nd , these contributions apparently merge into a single peak in C_p and thermal expansion³³ for smaller R . Also, judging from the shape of C_p/T , the onset of excess contribution for each R starts at a temperature close to T_{onset} in Fig. 1. For $R=\text{Gd}$ and Lu , integrating the excess C_p/T through the extrapolated

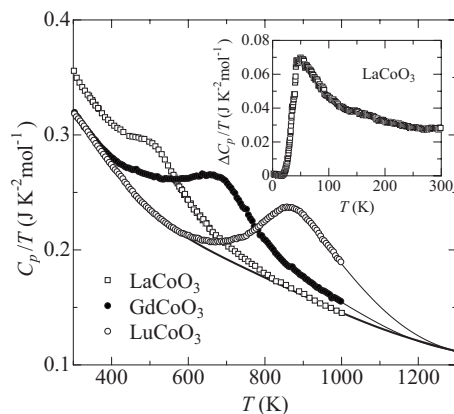


FIG. 4. Heat capacity divided by temperature for $R=\text{La}$, Gd , and Lu . The thick line shows the estimated baseline, while the thin lines are the extrapolated values for $R=\text{Gd}$ and Lu . The inset shows the low-temperature excess contribution for $R=\text{La}$, reproduced from Ref. 3.

C_p/T values (thin lines) gives 21 and 20 J K⁻¹ mol⁻¹, respectively, which are significantly smaller than the corresponding value for $R=\text{La}$.

A successful interpretation of the C_p data must explain the merging of spin-state and IM transition anomalies for small R , as well as the concomitant decrease in the entropy. Especially, these features are not likely to be described by a homogeneous Mott IM transition^{16,35} or successive spin-state transitions in the localized picture,⁶ as the phase diagram suggests that the number of excited spins at T_{IM} varies significantly with R . With these points in mind, we recall that configuration fluctuations between the LS and excited HS states of neighboring Co³⁺ ions could stabilize a metallic IS state via $t_{2g}^6 e_g^0 + t_{2g}^4 e_g^2 = 2t_{2g}^5 \sigma^{*1}$.^{13,34} For the e_g electrons to become itinerant, T must be high enough that the fluctuation rate becomes fast relative to the period of oxygen vibrations; this is indeed satisfied, as the reported frequencies of bending and stretching Co-O modes correspond to $\sim 450\text{--}900$ K,³⁶ in agreement with T_{IM} . Although previous discussions on $R=\text{La}$ assumed 50:50 ratio of HS and LS states at T_{IM} ,^{13,34} this mechanism could trigger an IM transition at lower HS concentrations if T is high enough to stabilize the itinerant state. Moreover, the transition leads to a fully metallic, homogeneous IS state that is consistent with both the band-structure calculations⁸ and transport measurements.^{7,35} (Band-structure calculations predict the IS state to be a metal and the LS and HS states to be insulators.) Below, we employ these ideas to provide one scenario for the explanation of the C_p anomalies and electronic phase diagram of $R\text{CoO}_3$.

The broad peak at the IM transition is reminiscent of the C_p anomaly due to the formation of ferroelectric nanoregions in relaxor ferroelectrics³⁷ and is consistent with the inhomogeneous mixed-spin state for the paramagnetic insulator phase. For $R=\text{La}$, the large T interval between T_{onset} and T_{IM} leads to the separation of C_p peaks for the spin-state transition and IM transition. Also, the spin-state excitations at low T increase the lattice constant and lattice C_p , leading to the

additional C_p contributions that can be regarded as due to spin-state-phonon coupling and that can explain the enhanced excess entropy found in $R=\text{La}$. For smaller R , the spin-state transition starts at higher T where the metallic state can be stabilized with a smaller increase in T . This leads to the continuous evolution from the onset of spin-state transition to the metallic IS state, resulting in the appearance of a single anomaly in C_p . As both the LS and excited-spin lattice C_p approach the same classical value above room temperature (the Debye temperature⁵ is ~ 600 K), the spin-state-phonon coupling becomes negligible for small R . It should be noted that the excess entropy found in $R=\text{Gd}$ and Lu is close to the value expected for the IS state, which is $R \ln 9 = 18.3$ J K⁻¹ mol⁻¹.^{5,38} Finally, while a larger bandwidth facilitates the IM transition, a critical number of excited spins is also needed for the configuration fluctuations to promote the IM transition; this could explain the evolution of T_{IM} that increases more strongly for small r_R compared to both T_{onset} and W^{-1} . Although these discussions do not completely rule out other possible models on the IM transition, the homogeneous IS metallic model appears to provide good explanation for many aspects of the present results.

IV. CONCLUSION

In conclusion, the evolution of spin-state and IM transitions has been clarified for $R\text{CoO}_3$ perovskites. It has become clear that a comprehensive theory of the transitions must also explain the phase diagram; the present results should be useful in guiding further theoretical efforts.

ACKNOWLEDGMENTS

We are grateful to T. Kyômen for helpful discussions and providing the heat capacity data of $R=\text{La}$. We also thank K. Asai, T. Shimoyama, and Y. Kuroiwa for valuable discussions. This study was supported by Special Coordination Funds from MEXT, Japan. The experiment at SPring-8 has been carried out with the approval of JASRI.

¹J. B. Goodenough, *J. Phys. Chem. Solids* **6**, 287 (1958).

²J.-Q. Yan, J.-S. Zhou, and J. B. Goodenough, *Phys. Rev. B* **69**, 134409 (2004).

³T. Kyômen, Y. Asaka, and M. Itoh, *Phys. Rev. B* **71**, 024418 (2005); **67**, 144424 (2003).

⁴C. Zobel, M. Kriener, D. Bruns, J. Baier, M. Grüninger, T. Lorenz, P. Reutler, and A. Revcolevschi, *Phys. Rev. B* **66**, 020402(R) (2002).

⁵S. Stølen, F. Grønvold, H. Brinks, T. Atake, and H. Mori, *Phys. Rev. B* **55**, 14103 (1997); *J. Chem. Thermodyn.* **30**, 365 (1998).

⁶K. Asai, A. Yoneda, O. Yokokura, J. M. Tranquada, G. Shirane, and K. Kohn, *J. Phys. Soc. Jpn.* **67**, 290 (1998).

⁷Y. Kobayashi, S. Murata, K. Asai, J. M. Tranquada, G. Shirane, and K. Kohn, *J. Phys. Soc. Jpn.* **68**, 1011 (1999).

⁸M. A. Korotin, S. Y. Ezhov, I. V. Solovyev, V. I. Anisimov, D. I. Khomskii, and G. A. Sawatzky, *Phys. Rev. B* **54**, 5309 (1996).

⁹P. G. Radaelli and S.-W. Cheong, *Phys. Rev. B* **66**, 094408

(2002).

¹⁰S. Noguchi, S. Kawamata, K. Okuda, H. Nojiri, and M. Motokawa, *Phys. Rev. B* **66**, 094404 (2002); Z. Ropka and R. J. Radwanski, *ibid.* **67**, 172401 (2003).

¹¹M. W. Haverkort, Z. Hu, J. C. Cezar, T. Burnus, H. Hartmann, M. Reuther, C. Zobel, T. Lorenz, A. Tanaka, N. B. Brookes, H. H. Hsieh, H.-J. Lin, C. T. Chen, and L. H. Tjeng, *Phys. Rev. Lett.* **97**, 176405 (2006).

¹²A. Podlesnyak, S. Streule, J. Mesot, M. Medarde, E. Pomjakushina, K. Conder, A. Tanaka, M. W. Haverkort, and D. I. Khomskii, *Phys. Rev. Lett.* **97**, 247208 (2006).

¹³J. B. Goodenough, *J. Alloys Compd.* **262-263**, 1 (1997).

¹⁴J. Baier, S. Jodlauk, M. Kriener, A. Reichl, C. Zobel, H. Kierspel, A. Freimuth, and T. Lorenz, *Phys. Rev. B* **71**, 014443 (2005).

¹⁵G. Demazeau, M. Pouchard, and P. Hagenmuller, *J. Solid State Chem.* **9**, 202 (1974).

¹⁶S. Yamaguchi, Y. Okimoto, and Y. Tokura, *Phys. Rev. B* **54**,

- R11022 (1996).
- ¹⁷J. A. Alonso, M. J. Martínez-Lope, C. de la Calle, and V. Pomjakushin, *J. Mater. Chem.* **16**, 1555 (2006).
- ¹⁸S. C. Mraw, in *Specific Heat of Solids*, edited by C. Y. Ho (Hemisphere, New York, 1988).
- ¹⁹T. Yoshida *et al.* (unpublished).
- ²⁰F. Izumi and T. Ikeda, *Mater. Sci. Forum* **321-324**, 198 (2000).
- ²¹M. Tachibana, T. Shimoyama, H. Kawaji, T. Atake, and E. Takayama-Muromachi, *Phys. Rev. B* **75**, 144425 (2007).
- ²²Full discussion on the crystal structure will be made elsewhere.
- ²³H. W. Brinks, H. Fjellvåg, A. Kjekshus, and B. C. Hauback, *J. Solid State Chem.* **147**, 464 (1999).
- ²⁴A. P. Sazonov, I. O. Troyanchuk, V. V. Sikolenko, G. M. Chobot, and H. Szymczak, *J. Phys.: Condens. Matter* **17**, 4181 (2005).
- ²⁵J.-S. Zhou and J. B. Goodenough, *Phys. Rev. Lett.* **94**, 065501 (2005).
- ²⁶T. Vogt, J. A. Hriljac, N. C. Hyatt, and P. Woodward, *Phys. Rev. B* **67**, 140401(R) (2003).
- ²⁷J.-S. Zhou, J.-Q. Yan, and J. B. Goodenough, *Phys. Rev. B* **71**, 220103(R) (2005).
- ²⁸M. Medarde, P. Lacorre, K. Conder, F. Fauth, and A. Furrer, *Phys. Rev. Lett.* **80**, 2397 (1998).
- ²⁹M. Marezio, J. P. Remeika, and P. D. Dernier, *Acta Crystallogr., Sect. B: Struct. Crystallogr. Cryst. Chem.* **26**, 2008 (1970); M. Marezio and P. D. Dernier, *Mater. Res. Bull.* **6**, 23 (1971).
- ³⁰M. T. Causa, R. D. Sánchez, M. Tovar, J. A. Alonso, and M. J. Martínez-Lope, *Phys. Rev. B* **68**, 024429 (2003).
- ³¹The bandwidth dependence of T_{IM} has been studied for $R = \text{La-Eu}$ in Ref. 28.
- ³²This baseline includes small contribution (expected to be $\sim 10\text{--}20 \text{ mJ K}^{-2} \text{ mol}^{-1}$) from metallic C_p at high T . The choice of baseline does not affect the difference in the excess entropy among various R .
- ³³K. Knížek, Z. Jirák, J. Hejtmánek, M. Veverka, M. Maryško, G. Maris, and T. T. M. Palstra, *Eur. Phys. J. B* **47**, 213 (2005).
- ³⁴M. A. Señarís-Rodríguez and J. B. Goodenough, *J. Solid State Chem.* **116**, 224 (1995); **118**, 323 (1995).
- ³⁵Y. Tokura, Y. Okimoto, S. Yamaguchi, H. Taniguchi, T. Kimura, and H. Takagi, *Phys. Rev. B* **58**, R1699 (1998).
- ³⁶S. Yamaguchi, Y. Okimoto, and Y. Tokura, *Phys. Rev. B* **55**, R8666 (1997); A. Ishikawa, J. Nohara, and S. Sugai, *Phys. Rev. Lett.* **93**, 136401 (2004).
- ³⁷Y. Moriya, H. Kawaji, T. Tojo, and T. Atake, *Phys. Rev. Lett.* **90**, 205901 (2003).
- ³⁸In an itinerant picture, one could argue that the excess entropy corresponds to a metallic contribution with an electronic C_p coefficient of $\sim 20 \text{ mJ K}^{-2} \text{ mol}^{-1}$.